Aging Strengthening Mechanism of the Cu-1.0Zr Alloy

KA TIAN, BAOHONG TIAN, YI ZHANG, YONG LIU, and ALEX A. VOLINSKY

The effects of different aging processes on electrical conductivity and microhardness of a Cu-1.0Zr alloy were investigated. Microstructure and precipitates of the aged alloy were analyzed by transmission electron microscopy, and the aging strengthening mechanism of the Cu-1.0Zr alloy is discussed. Good comprehensive performance of the Cu-1.0Zr alloy can be obtained by aging at 773K (500 °C) for 1 hour, for which electrical conductivity reached 80.2 pct IACS, while microhardness reached 155.6 HV. Small amounts of a Zr-rich phase and annealing twins were present in the solid solution. A large amount of 3-18 nm $Cu_{10}Zr_7$ precipitates were present in the copper matrix. At the early stage of aging, the precipitates were small and their density was relatively low. As aging time progressed, the precipitates gradually increased in size. After overaging, the precipitated phase was dissolved, resulting in reduced microhardness. After aging at 723 K (450 °C) for 6 hours, the precipitates were $Cu_{10}Zr_7$. The peak Cu-1.0Zr alloy performance was achieved after aging at 773 K (500 °C) for 1 hour, and the main reason for the performance increase is coherent strain hardening.

DOI: 10.1007/s11661-017-4292-6

I. INTRODUCTION

COPPER alloys can be strengthened by aging, resulting in high strength and electrical conductivity, along with adequate thermal conductivity. Copper alloys are widely used in electrical switching contact bridges, as separation rings, coal-fired power plant burner nozzles, and spot welding electrodes.[1–3] According to the Cu-Zr binary phase diagram,[4] the maximum solid solubility of Zr in Cu is 0.15 pct at 1239 K (966 °C). Furthermore, the solubility of Zr in Cu decreases rapidly with decreasing temperature. In many studies the amount of Zr was between 0.05 pct and 0.3 pct, which is near or greater than the maximum solubility. Purcek *et al*. studied optimization of strength, ductility, and electrical conductivity of the Cu-Cr-Zr alloy by combining multi-route equal-channel angular pressing and aging, where Zr content was 0.08 pct.[5] Chatterjee *et al*. studied damage in thermally fatigued Cu-Cr-Zr alloy, where Zr content was 0.1 pct.[6] Deng *et al*. studied microstructure and physical properties of powder metallurgy Cu-Zr alloys, and the Zr content was 0.1 pct.[7] Jiang *et al*. studied pre-deformation and aging characteristics of the Cu-Te-Zr alloy with Zr content of 0.2 pct.[8] In this study, the Zr content of the Cu-Zr alloy was selected at 1 pct, which is far higher than its maximum solid solubility. Excess Zr is supposed to form secondary phases, resulting in enhanced material properties. The Cu-Zr alloy was treated at a high temperature, developing a supersaturated solid solution. After aging, decomposition of the supersaturated solid solution produced a large number of precipitates to obtain high strength and high conductivity of copper alloys.[9]

At present, there are three main mechanisms of precipitation phase strengthening: coherent strain strengthening, dislocation shear strengthening, and the Orowan dislocation bypassing strengthening mechanisms. Wang *et al*.[10] believe that the Cu-0.75Cr-0.13Zr alloy conforms to the Orowan dislocation bypassing strengthening mechanism. Watanabe *et al*.[11] also think that Cu-Cr alloy is consistent with the Orowan dislocation bypassing strengthening mechanism. However, Liu *et al*.[12] think that rapid solidification of the Cu-Cr alloy is in accordance with the coherent strain strengthening mechanism. Nevertheless, Holzwarth *et al*.[13] deemed that Cu-Cr-Zr is more suitable for the Orowan dislocation bypassing strengthening mechanism by comparing it with the coherent strain strengthening mechanism. The precipitation strengthening effect in Cu-Zr alloys is very small. In this paper, the newly developed high Zr content Cu-1.0Zr alloy was studied by performing solid solution and aging treatments. The

KA TIAN, BAOHONG TIAN, YI ZHANG, and YONG LIU are with the School of Materials Science and Engineering, Henan University of Science and Technology, Luoyang 471023, China, and also with the Collaborative Innovation Center of Nonferrous Metals, Luoyang, 471023, Henan Province, China. Contact e-mail: tianka123@163.com ALEX A. VOLINSKY is with the Department of Mechanical Engineering, University of South Florida, Tampa FL 33620. Contact e-mail: volinsky@usf.edu

Manuscript submitted December 11, 2016.
Article published online August 24, 2017

alloy performance was assessed using microanalysis to study the strengthening mechanism.

II. EXPERIMENTAL DETAILS

The experimental alloy was melted in a vacuum induction furnace under argon atmosphere by using 99.95 wt pct standard cathode copper Cu-CATH-2, Zr blocks with 99.5 pct purity, which were cast into low carbon steel molds with 80 mm × 150 mm dimensions. The Cu-1.0Zr alloy was extruded into 33 mm diameter rods using a XJ-500 extrusion machine. The extruded rods were solution-treated at 1173 K (900 °C) for 1 hour, followed by water quenching. Then, the solid solution of Cu-1.0Zr alloy was cut into 100 mm × 5 mm × 1 mm strips. After cutting, 60 pct cold deformation was carried out on a C33150-type laminating machine. The electrical resistance of the specimens was measured using a ZY9987 digital micro ohm meter. The measurement length of the specimen was larger than 70 mm, and the measurement error was less than 0.02 mΩ. Each sample was measured at least 3 times, and the average conductivity value was taken. Microhardness was measured using an HV1000 microhardness tester, with a load of 100 g and a loading time of 10 seconds. Each specimen was tested 5 times, and the microhardness measurement error is within ±5 pct.

TEM samples were prepared using a DJ2000 twin jet electropolishing instrument. The electrolyte solution was HNO_3:C_2H_5OH = 1:4. The small angle of the sample was thinned by a Gatan 691 ion thinning instrument. The ion beam incident angle was 5 deg, the ion beam energy was 4 keV, and the ion milling time was 30 minutes. Microstructure and precipitated phase of the alloy were analyzed by a JEM-2100 high-resolution transmission electron microscope operated at 200 kV accelerating voltage.

III. RESULTS AND DISCUSSION

A. *Performance and Microstructure*

Figure 1(a) shows the relationship between the conductivity and the aging time of the Cu-1.0Zr alloy after 60 pct cold deformation. Scattered solid solution atoms in the copper matrix significantly affect electrical conductivity of the Cu-1.0Zr alloy.[14,15] At 673 K (400 °C), 723 K (450 °C), 773 K (500 °C), and 823 K (550 °C), the conductivity change trend is basically the same. In the early aging stage (0-1 hour), conductivity increases rapidly. With increasing aging time (1-6 hours), however, conductivity becomes constant or increases slowly. Solid solution conductivity of the Cu-1.0Zr alloy is 57.2 pct IACS. After aging for 1 hour at 673 K (400 °C), 723 K (450 °C), 773 K (500 °C), and 823 K (550 °C), electrical conductivity was 70.1 pct IACS, 73.3 pct IACS, 80.2 pct IACS, and 84.4 pct IACS. Compared with the solid solution, electrical conductivity increased by 22.6, 28.1, 40.2, and 47.6 pct, respectively. Increasing aging time from 1 hour to 6 hours at 673 K (400 °C), 723 K (450 °C), and 773 K (500 °C) resulted in conductivity slowly increasing by 5.4 pct (70.1-73.9 pct IACS), 9.8 pct (73.3-80.5 pct IACS), and 3.2 pct (80.2-82.8 pct IACS). However, when the alloy was aged at 823 K (550 °C), conductivity slightly changed between 1 hour and 6 hours aging. Maximum conductivity change was 0.8 pct (84.5-85.2 pct IACS). In the early aging stage, the matrix has a high degree of over-saturation with secondary phase precipitation. The precipitation rate of the secondary phase is relatively fast, so the alloy conductivity increases rapidly. With longer aging time (1-6 hours), the amount of solid solution elements in the matrix will decrease. The rate of the secondary phase precipitation will become slower, resulting in constant electrical conductivity. The increase of aging temperature enhances the diffusion rate of the solid solution atoms and accelerates the precipitation rate of the secondary phase. As the aging time is prolonged, the solid solution elements in the matrix continue to precipitate, which causes continued increase in conductivity. However, when the content of solid solution element in the matrix decreases, the secondary phase precipitation rate slows down, so the rate of conductivity increase slows down.

Figure 1(b) shows the relationship between microhardness and aging time for the Cu-1.0Zr alloy after 60 pct cold deformation. It can be seen from Figure 1(b) that at the beginning of aging, the aging temperature provides the driving force for the precipitation of the secondary phase, and thus microhardness increases rapidly.[16] At 673 K (400 °C), due to lower aging temperature, the atoms diffuse slowly. Accordingly, precipitation is slow and stable. Thus, the microhardness maintained an upward trend. As the aging temperature increases, the secondary phase precipitation rate is accelerated, and the alloy shows a peak in microhardness at 723 K (450 °C), 773 K (500 °C), and 823 K (550 °C), at the peak time of 2 hours, 1 hour, and 0.5 hours, respectively. The highest microhardness is 159.1 HV, 155.6 HV, and 143.1 HV. The higher the temperature, the shorter the time to reach the peak value with smaller peak hardness. Based on Figure 1, the Cu-1.0Zr alloy has the best properties after aging at 773 K (500 °C) for 1 hour, where conductivity reaches 80.2 pct IACS and hardness reaches 155.6 HV.

The microstructure of the Cu-1.0Zr alloy after solid solution treatment at 900 °C for 1 hour is shown in Figure 2. The Cu-1.0Zr alloy after solid solution treatment has a large number of equiaxed grains, and a small amount of annealing twins is produced. The formation of twins is closely related to the stacking faults. The stacking fault energy of Cu is relatively low, which makes it easy to produce twins. The interface energy is very low, and coherent twin boundaries are observed along a straight line under the microscope. This mean free path through the twin boundary is reduced, resulting in higher dislocation density and a hardening effect. Figure 3 shows a scanning electron microscopy image and energy spectrum analysis of the Cu-1.0Zr alloy after solid solution treatment at 900 °C for 1 hour. There is an insoluble particle in the matrix, which is the Zr-rich phase, according to EDS analysis. The amount

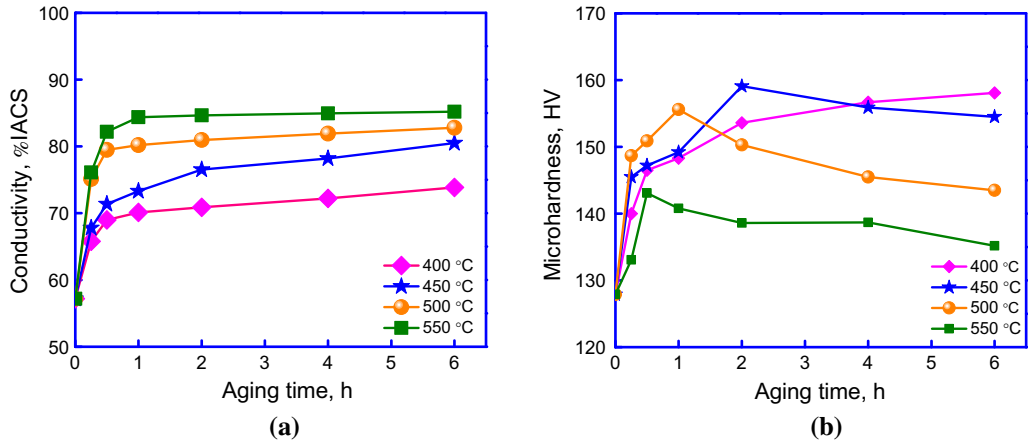

Fig. 1—Conductivity and microhardness of the Cu-1.0Zr alloy as a function of aging time under different aging temperatures: (*a*) conductivity; (*b*) microhardness.

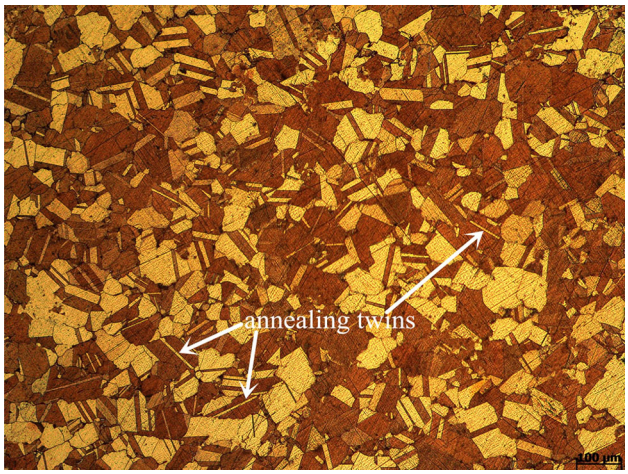

Fig. 2—Microstructure of the Cu-1.0Zr alloy after solution treatment at 1173 K (900 °C) for 1 h.

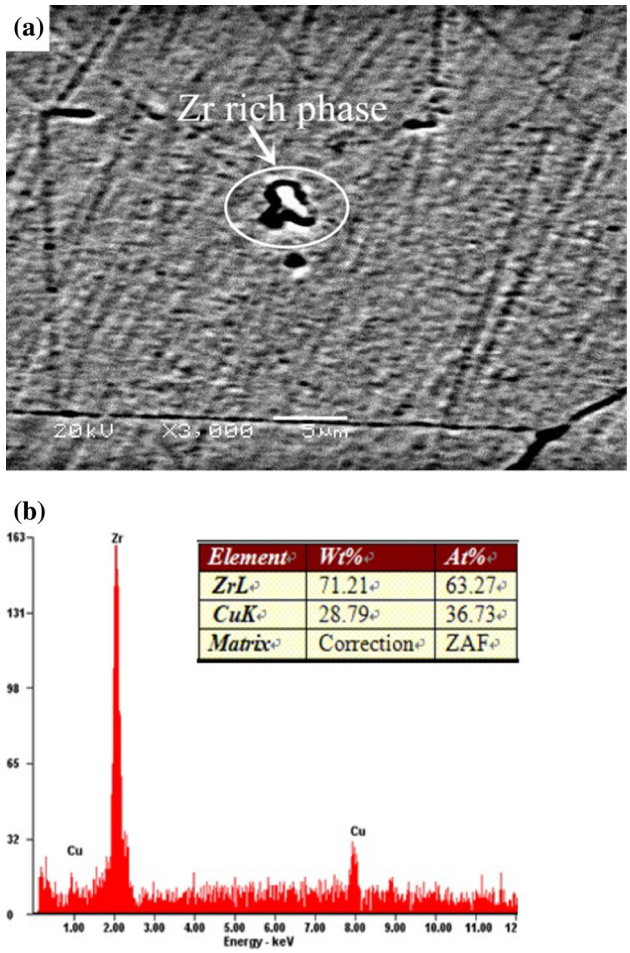

Fig. 3—(*a*) SEM micrograph of the Cu-1.0Zr alloy after solution treatment at 1173 K (900 °C) for 1 h and (*b*) corresponding EDS analysis.

of added Zr was more than the maximum solid solubility of Zr, so it did not completely dissolve in the Cu matrix. Figure 4 shows the microstructure of the solid solution Cu-1.0Zr alloy obtained by transmission electron microscopy. A large number of precipitated phase particles are dispersed in the matrix, and their size is 3-18 nm. The diffraction pattern corresponds to the $Cu_{10}Zr_7$ phase.

Figure 5 shows TEM images of Cu-1.0Zr alloy after 60 pct cold deformation under different conditions. It can be seen from Figure 5(a) that the precipitates are dispersed in the copper matrix after aging at 723 K (450 °C) for 1 hour. The precipitates are small and their density is low, which indicates that the decomposition of the solid solution is not sufficient. The number of precipitates gradually increased with aging time. As seen in Figure 5(b), a large amount of precipitates is dispersed in the copper matrix after aging at 723 K (450 °C) for 6 hours. Comparison with Figures 5 (b), 5(c) shows that the precipitates have obviously coarsened and their density decreased. It also shows that re-dissolution of solute atoms occurred in the coarsening process. The Cu-1.0Zr alloy aged at 823 K (550 °C) for 6 hours has been overaged and the precipitated phase became coarser, so the microhardness of the alloy aged

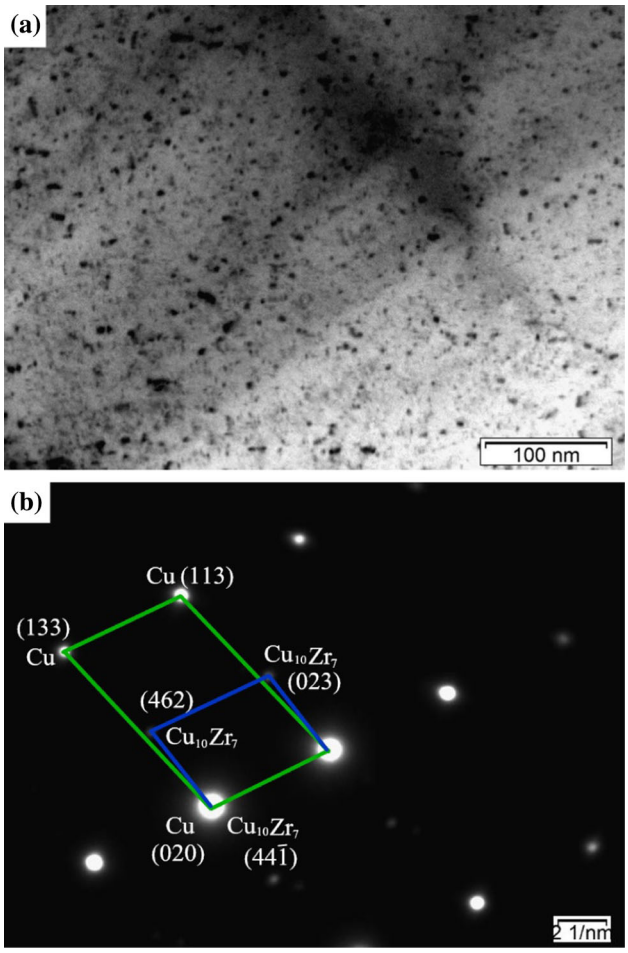

Fig. 4—(*a*) TEM micrographs of the Cu-1.0Zr alloy after solution treatment and (*b*) corresponding indexed SAED pattern.

at 723 K (450 °C) for 6 hours is higher than the one aged at 823 K (550 °C) for 6 hours in Figure 1.

Figure 6 shows TEM images after 60 pct cold deformation of the Cu-1.0Zr alloy aged at 723 K (450 °C) for 6 hours. There are dispersion phases present in the matrix. From selected area electron diffraction (SAED) pattern and indexing, the precipitates are identified as $Cu_{10}Zr_7$, shown in Figure 6(b). One can see the Moire fringes in the high-resolution TEM image shown in Figure 6(c). Precipitates cause lattice mismatch, producing elastic stress fields, which can also improve the alloy strength.

The precipitated phase is $Cu_{10}Zr_7$ in this article. However, there are many different opinions about the types of precipitates. Mu *et al.*[17] believe that the Cu-Cr-Zr-Mg-RE alloy has a zirconium-rich phase at 723 K (450 °C). Su *et al.*[18] think that the precipitated phase is Cu_5Zr in the Cu-Cr-Zr alloy aged at 773 K (500 °C) for 30 minutes. Xie *et al.*[19] believe that Cu_4Zr precipitates are nucleated preferentially at the pre-nucleated Cr particles in the Cu-Cr-Zr-Sn alloy, and are semi-coherent with the matrix. Kawakatsu *et al.*[20] think that the precipitate of Cu-Cr-Zr alloy is Cu_3Zr. Deng *et al.*[7] believe that in the Cu-0.1 pctZr alloy prepared by the powder metallurgy method, the Cu_2Zr phase precipitated after solid solution aging treatment. Huang *et al.*[21] analyzed the microstructure of the Cu-0.31Cr-0.21Zr alloy and concluded that the precipitated phase was $Cu_{51}Zr_{14}$. Saitoh *et al.*[22] studied microstructure formed by the eutectic reaction of the Cu-Zr alloy with a Zr concentration of 12.3 wt pct and the precipitated phase was Cu_9Zr_2. The precipitated phase is $Cu_{10}Zr_7$ and its eutectic temperature is 1168 K (895 °C),[20] while the solid solution treatment temperature is 1173 K (900 °C). The solution temperature and eutectic temperature are almost the same and higher Zr content addition results in $Cu_{10}Zr_7$ precipitation.

B. *Strengthening Mechanism Discussion*

The aging strengthening mechanism can be explained by the dislocation theory. During the aging process, dislocations motion is hindered due to the precipitated phase, resulting in a strengthening effect. There are three main types of alloy precipitation strengthening mechanisms. They are the coherent strain hardening, dislocation shear strengthening, and the Orowan dislocation strengthening mechanisms. Due to the difference in alloy composition and aging process parameters, the structure of precipitated phase and the relationship between the matrix and precipitated phase are different, producing different strengthening mechanisms. The strengthening mechanism can be one or a combination of several mechanisms. At different stages of aging, the role of strengthening mechanisms is different. Strength and hardness of the Cu-1.0Zr alloy are greatly improved by aging treatment. The microhardness of the alloy aged at 773 K (500 °C) for 1 hour reached the maximum value. The degree of lattice mismatch is 0.54 pct, and there is a coherent relationship between the precipitation and the matrix. The shear stress increment caused by the coherent strain hardening of the Cu-1.0Zr alloy after aging is[23]

$$\Delta\tau = X(\varepsilon G)^{\frac{3}{2}}(rfb/F)^{\frac{1}{2}}. \quad [1]$$

Here, ε is the misfit strain parameter, G is the shear modulus of the matrix, r is the average radius of the precipitates, f is their volume fraction, b is the matrix Burgers vector, and F is the line tension of a dislocation being pinned by the precipitates. The parameter X varies depending on the theory used, and is assumed to range from 2 to 3. Following Ardell,[24] $X = 2.6$ and $F = \alpha G b^2$, with α ranging from 0.089 to 0.5.

Gerold and Haberkovn[25] used isotropic elastic theory to calculate the maximum interaction of coherent precipitates and edge type dislocation line Fm

$$F_m = 4Gb\varepsilon r. \quad [2]$$

When two dislocation segments meet the condition when the cosine of the angle $\cos(\psi_c/2) = Fm/2F = 1$,[26] one can find the maximum shear radius of the coherent precipitate:

$$r_{\max} = F/2Gb\varepsilon. \quad [3]$$

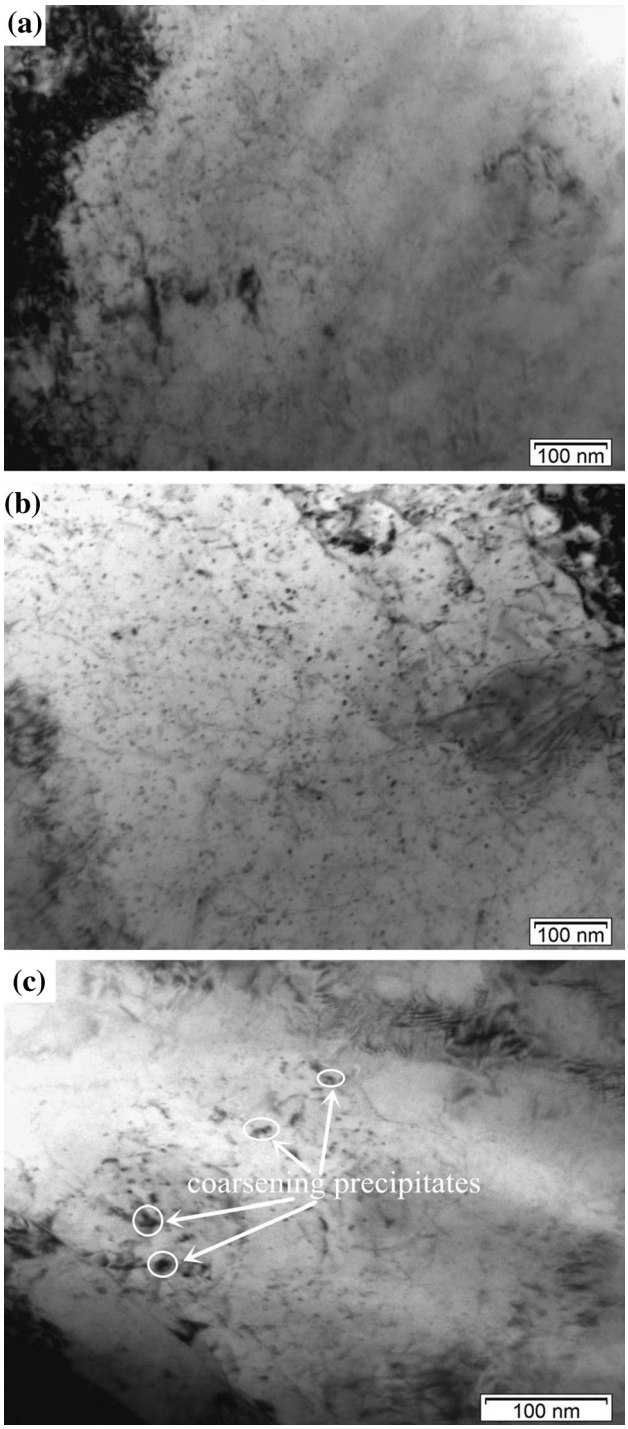

Fig. 5—TEM micrographs of the Cu-1.0Zr alloy under different conditions: (*a*) 723 K (450 °C) aging for 1 h; (*b*) 723 K (450 °C) aging for 6 h; (*c*) 823 K (550 °C) aging for 6 h.

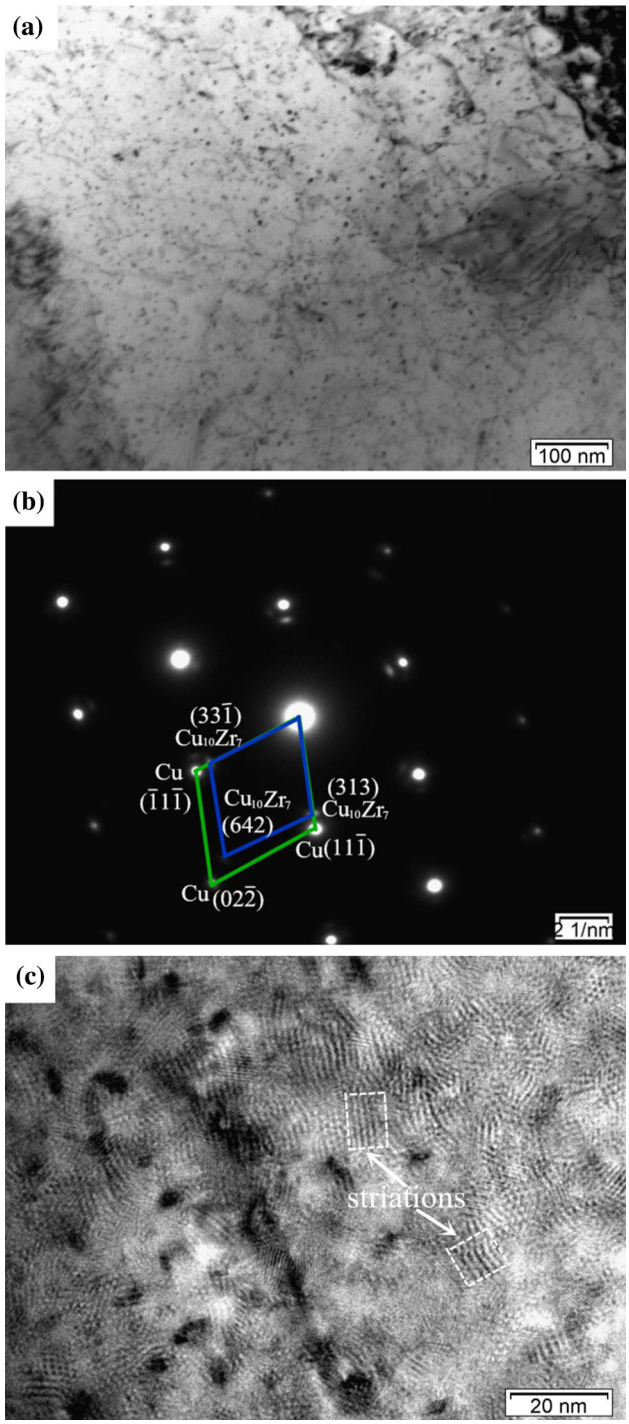

Fig. 6—TEM micrographs and SAED pattern of the Cu-1.0Zr alloy after 60 pct cold rolling and 723 K (450 °C) aging for 6 h: (*a*) TEM micrograph; (*b*) indexed SAED pattern; (*c*) HRTEM micrograph of the precipitates.

By placing Eq. [3] into Eq. [1], the estimated maximum shear stress caused by the coherent strain hardening is obtained:

$$\Delta\tau_{max} = 1.84G\varepsilon f^{\frac{1}{2}} \qquad [4]$$

Figure 7 shows TEM images and the inverse Fourier transform of the Cu-1.0Zr alloy cold-rolled to 60 pct and aged at 773 K (500 °C) for 1 hour. Figure 7(a) shows the Cu-1.0Zr alloy precipitates distributed in the copper matrix. Figure 7(b) shows a high-resolution

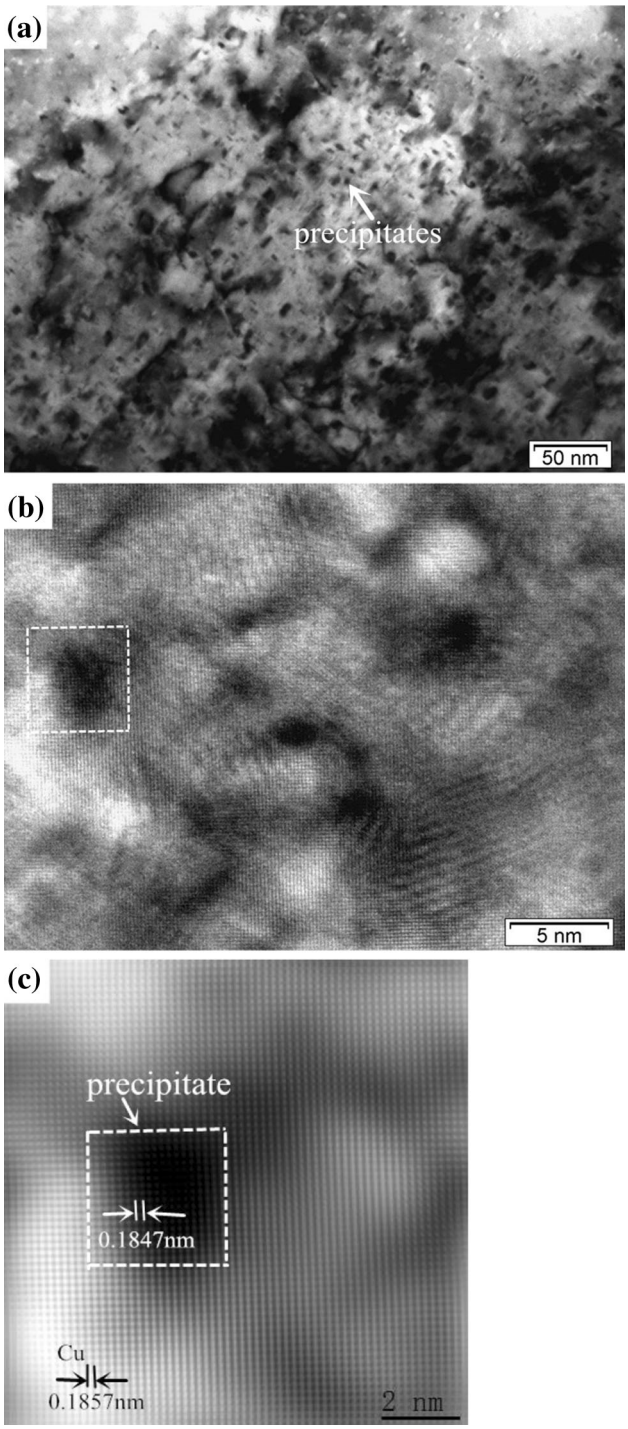

Fig. 7—TEM image of the Cu-1.0Zr alloy after 60 pct cold rolling and 773 K (500 °C) aging for 1 h: (*a*) precipitates; (*b*) HRTEM image; (*c*) inverse FFT.

TEM (HRTEM) image of the precipitated phase. The HRTEM images of the white section were subjected to inverse Fourier transform, showing atoms of the precipitated phase and Cu matrix atoms. A distance of 10 atoms is measured at one time, and the average value is obtained after 10 measurements. Under the same conditions, the 2 nm distance between 10 atoms is measured under HRTEM. Calculated distance between the precipitated atoms is 0.1847 nm, while the calculated distance between the Cu atoms is 0.1857 nm. The misfit degree is 0.54 pct. According to Eshelby,[27] $\varepsilon = \frac{2}{3}\delta = 0.36$ pct. By placing $G = 44.1$ GPa and$\varepsilon = 0.36$ pct into Eq. [4], the increment of maximum intensity value generated by the coherent strain hardening precipitated phase is obtained:

$$\Delta\sigma_{\max} = 292f^{\frac{1}{2}}. \quad [5]$$

Here, f is the volume fraction of the coherent precipitated phase.

When Cu-1.0Zr alloy was aged at 773 K (500 °C) for 1 hour, the volume fraction of the precipitated phase was $f = 89.8$ pct. When using this value in Eq. [5], the calculated maximum tensile strength increment is 276 MPa. This value plus the tensile strength of the as-cast copper (197 MPa) is 473 MPa, which is very close to the tensile strength 465 MP of the corresponding peak performance condition. Therefore, for the Cu-1.0Zr alloy aged at 773 K (500 °C) for 1 hour, the coherent strain hardening mechanism is the main contributor to alloy strengthening.

IV. CONCLUSIONS

Good comprehensive performance of the Cu-1.0Zr alloy was obtained after solid solution treatment at 1173 K (900 °C) for 1 hour and aging at 773 K (500 °C) for 1 hour. Electrical conductivity reached 80.2 pct IACS and microhardness reached 155.6 HV. There is a small amount of the Zr-rich phase and annealing twins present in the solid solution state. At 723 K (450 °C), the amount of precipitated phase gradually increases with aging time. When overaged at 823 K (550 °C) for 6 hours, the precipitates cause coarsening. There is a large amount of $Cu_{10}Zr_7$ precipitates present after aging at 723 K (450 °C) for 6 hours. The Cu-1.0Zr alloy reaches the maximum strength after aging at 773 K (500 °C) for 1 hour. The strength value estimated by the coherent strain hardening mechanism is close to the experimentally observed value.

ACKNOWLEDGMENTS

This work was supported by the National Natural Science Foundation of China (51101052) and the Science and Technology Innovation Talents in Universities of the Henan Province (14IRTSTHN007) and by the National Science Foundation (IRES 1358088).

REFERENCES

1. Z.Y. Pan, J.B. Chen, and J.F. Li: *Trans. Nonferrous Met. Soc. China*, 2015, vol. 4, pp. 1206–14.
2. Y. Zhang, Z. Chai, A.A. Volinsky, B.H. Tian, H.L. Sun, P. Liu, and Y. Liu: *Mater. Sci. Eng., A*, 2016, vol. 662, pp. 320–29.

3. S.G. Jia, J.B. Chen, X.H. Chen, B.H. Tian, and F.Z. Ren: *Chin. J. Nonferrous Met.*, 2010, vol. 20, pp. 1334–38.
4. H. Okamoto: *J. Phase Equilib. Diffus.*, 2008, vol. 29, p. 204.
5. G. Purcek, H. Yanar, M. Demirtas, Y. Alemdag, D.V. Shangina, and S.V. Dobatkin: *Mater. Sci. Eng., A*, 2016, vol. 649, pp. 114–22.
6. A. Chatterjee, R. Mitra, A.K. Chakraborty, C. Rotti, and K.K. Ray: *J. Nucl. Mater.*, 2016, vol. 474, pp. 120–25.
7. J.Q. Deng, Y.C. Wu, F.W. Yu, and D.G. Wang: *Rare Metal Mater. Eng.*, 2009, vol. 38, pp. 205–08.
8. L. Jiang, F. Jiang, C. Dai, X. Wang, and W. Zong: *Chin. J. Nonferrous Met.*, 2010, vol. 20, pp. 878–84.
9. N. Bai, Y.M. Zhang, K.X. Song, N.N. Li, and X. He: *Heat Treat. Met.*, 2015, vol. 40, pp. 103–06.
10. K. Wang, K.F. Liu, and J.B. Zhang: *Rare Met.*, 2014, vol. 33, pp. 134–38.
11. C. Watanabe, R. Monzen, and K. Tazaki: *J. Mater. Sci.*, 2008, vol. 43, pp. 813–19.
12. P. Liu, B.X. Kang, X.G. Cao, J.L. Huang, and H.C. Guo: *Acta Merallurgica Sinica*, 1999, vol. 35, pp. 561–64.
13. U. Holzwarth and H. Stamm: *J. Nucl. Mater.*, 2000, vol. 279, pp. 31–45.
14. J.B. Correia, H.A. Davies, and C.M. Sellars: *Acta Mater.*, 1997, vol. 45, pp. 177–90.
15. M. Deng, S.G. Jia, P.P. Zhao, M.J. Wang, J.B. Dang, C. Duan, and X. Yu: *Trans. Mater Heat Treat.*, 2013, vol. 34, pp. 67–69.
16. R.Q. Liu, W.B. Xie, G.J. Huang, J.B. Zhang, and G.B. Qiu: *Mater. Sci. Technol.*, 2015, vol. 23, pp. 124–28.
17. S.G. Mu, F.A. Guo, Y.Q. Tang, X.M. Cao, and M.T. Tang: *Mater. Sci. Eng. A*, 2008, vol. 475, pp. 235–40.
18. J.H. Su, P. Liu, Q.M. Dong, H.J. Liu, F.Z. Ren, and B.H. Tian: *Trans. Mater. Heat Treat.*, 2005, vol. 26, pp. 62–65.
19. H.F. Xie, X.J. Mi, G.J. Huang, B.D. Gao, X.Q. Yin, and Y.F. Li: *Rare Met. Mater. Eng.*, 2012, vol. 41, pp. 1549–54.
20. I. Kawakatsu, H. Suzuki, and H. Kitano: *J. Jpn. Inst. Met.*, 1967, vol. 31, pp. 1253–57.
21. F.X. Huang and J.S. Ma: *Scripta Mater.*, 2003, vol. 48, pp. 97–02.
22. M. Saitoh, M. Kajihara, Y. Tomioka, and J. Miyake: *J. Mater. Sci. Eng. A*, 2001, vol. 318, pp. 87–93.
23. V. Gerold: *North Holland*, 1979, vol. 45, pp. 499–500.
24. A.J. Ardell: *Metall. Trans. A*, 1985, vol. 16, pp. 2131–65.
25. V. Gerold and H. Haberkovn: *Phys. Status Solidi*, 1966, vol. 16, pp. 675–84.
26. N. Hanse: *Metall. Trans. A*, 1985, vol. 16, pp. 2167–90.
27. U. Holzwarth and H. Stamm: *J. Nucl. Mater.*, 2000, vol. 279, pp. 31–45.